2024 IEEE International Conference on Robotics and Automation (ICRA 2024)
May 13-17, 2024. Yokohama, Japan

Tip-Clutching Winch for High Tensile Force Application with Soft Growing Robots

O. Godson Osele†, Kentaro Barhydt†, Nicholas Cerone, Allison M. Okamura, and H. Harry Asada

***Abstract*— The navigational abilities of tip-everting soft growing robots, known as vine robots, are compromised when tip-mount devices are added to enable carrying of payloads. We present a new method for securing a vine robot to objects or its environment that exploits the unique eversion-based growth mechanism and flexibility of vine robots, while keeping the tip of the vine robot free of encumbrance. Our implementation is a tip-clutching winch, into which vine robots can insert themselves and anchor to via powerful overlapping belt friction. The device enables passive, high-strength, and reversible fastening, and can easily release the vine robot. This approach enables carrying of loads of at least 28 kg (limited by the tensile strength of the vine robot body material and winch actuator torque capacity), as well as novel material transport and locomotion capabilities.**

I. Introduction

Inflated soft growing robots, or "vine robots", have unique navigation benefits that enable them to reach places and achieve complex configurations. A vine robot achieves "growth" at its tip through pressure-driven eversion of flexible, thin-walled membranes, transferring material from inside its tubular body to the outside. This allows for navigation through cluttered environments without external surface friction, navigation through gaps much smaller than its width, and growth upwards against gravity due to its lightweight construction [1].

Another benefit of vine robots commonly discussed in literature [2] is their ability to apply pulling forces due to the inextensibility of their membrane material. Typical vine robots made from low-density polyethylene (LDPE) plastic have been shown to have high tensile pulling capacities of up to 25.5 kg [3]. Vine robots made from stronger materials like nylon fabrics [4], [5] show significant promise for achieving much higher tensile pulling capacities. This pulling functionality can enable new material transport applications in which the vine robot navigates its tip to a point in the environment, grasps it, and is reeled in to pull its base to that point while carrying a payload. Potential applications include deployable elevators or hoists, self-attaching pulling hitches, pulling payloads through rubble, and pipe inspection and cleaning. However, securely fastening the tip of the vine robot to objects to apply these pulling forces without inhibiting its navigation capabilities is a challenging problem because the everting robot body material is added to and removed from the tip during growth and retraction, respectively.

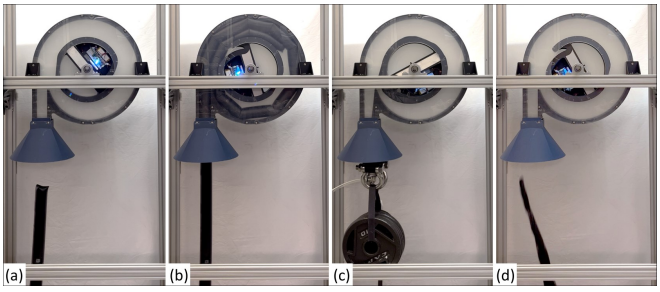

Fig. 1: Demonstration of the tip-clutching winch mechanism showing: (a) a vine robot entering the device and (b) navigating around the winch inside of the mechanism to assume the clutching configuration, (c) the mechanism securely clutching and pulling the vine robot to lift a high load, and (d) the vine robot falling out of the device after being unwound by the winch.

Various tip-mount devices have been developed to attach instrumentation and mechanisms to the tip of the vine robot while still allowing for growth [2], [3], [5]. These tip mounts are designed to stay at the tip while allowing everting or inverting membrane material to pass through them. However, tip mounts typically add mass and rigidity to the tip, introducing significant functional limitations. Their mass is often too large for the vine robots to lift off the ground, especially at long extensions. The tip mount size also sets the smallest gap that a vine robot can pass through. Additionally, the tensile load capacity of rigid tip mounts are typically lower than that of the vine robot body material. The highest tensile pulling load capacity demonstrated by a vine robot with a tip mount to date is only 2.5 kg [3]. The mass and size requirements of tip-mount devices, as well as the need to feed the vine robot body material through a tip mount, severely limit the load capacity of vine robots with tip mounts. The goal of this work is to achieve large pulling forces with vine robots by eliminating the tip mount and instead anchoring to the environment using friction within a novel tip-clutching winch (TCW) mechanism.

The tip-clutching winch is a device into which vine robots can insert themselves and anchor to via powerful overlapping belt friction. The device can also wind up the vine robot and achieve pulling forces that are at least an order of magnitude larger than prior work. The design of this device leverages the unique growth mechanism and flexibility of the vine robot to enable automatic, high-strength, and reversible fastening. The vine robot is only attached to the tip-clutching winch

†These authors contributed equally to this work and are co-first authors.

This work is supported in part by the Ford Foundation Predoctoral Fellowship, a Stanford SystemX Fellowship, National Science Foundation grant #2344314, and NSK Ltd.

KB, NC, and HHA are with the Department of Mechanical Engineering, MIT, Cambridge, MA, 02139 USA {kbarhydt, ceronj26, asada}@mit.edu

OGO and AMO are with the Department of Mechanical Engineering, Stanford University, Stanford, CA 94305 USA {obum, aokamura}@stanford.edu

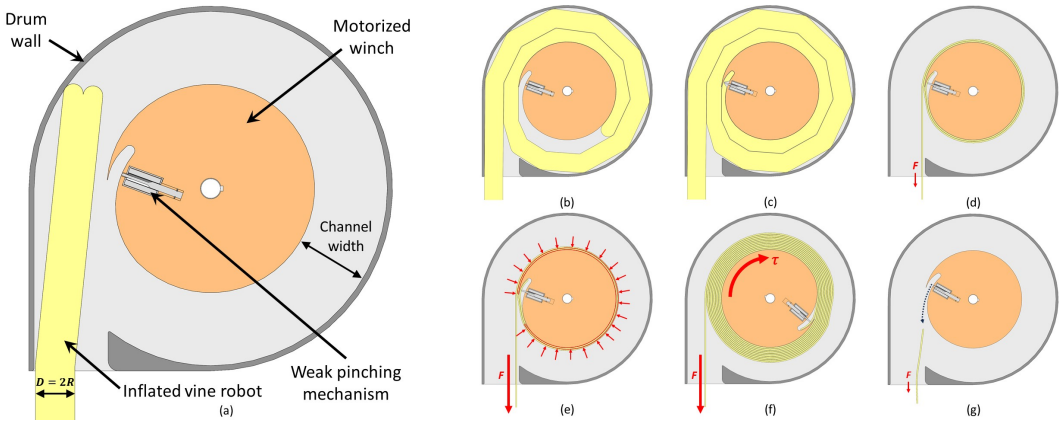

Fig. 2: Schematic and functional sequence of the vine robot tip clutching winch mechanism. The device consists of a drum outer housing, and a motorized winch with a tip slot and weak pinching mechanism. (a): The vine robot enters the drum and begins navigating around its inner wall. (b): The vine robot completes its first rotation around the winch and continues to grow the second inner layer through the space between the outer layer and winch. (c): The vine robot wraps completely around the winch and its tip grows into a slot in the winch, where it is pinched by a weak pinching mechanism. (d): The vine robot deflates and is tightened around the winch. (e): The tensile load tightens the vine robot and increases the wrapping pressure that the outer layer applied onto the inner layer, engaging the friction clutch. The pinching mechanism can now be disengaged. (f): The winch rotates to wind up the vine robot body further into the drum. (g): To disengage and release the vine robot, the winch simply unwinds it until the tensile load can pull it out of the drum.

device after its tip is purposefully engaged, and thus the winch does not hinder the vine robot's beneficial navigation abilities. (I.e., the device does not constrain the vine robot's path to the ground or limit how small of a gap it can enter.) This device design broadens the functionality of vine robots to fulfill their potential for applying high tensile pulling forces, and introduces new applications.

II. Mechanical Principles and Modeling

A. Mechanical Principles

The primary functions of the tip-clutching winch design are: (1) enable a simple vine robot to enter and automatically configure itself inside the device for secure attachment, and (2) engage, hold, retract, and disengage the vine robot while bearing heavy tensile loads. Two primary principles underlie our tip clutching device design to enable these functions.

The first principle is **obstacle-aided navigation**, which is the passive redirection of the vine robot tip growth due to collisions of its tip with the environment [6]. Our design employs this principle to enable the vine robot to navigate through the device into the desired securing configuration without active steering. The second principle is **overlapping belt friction** which is the use of multi-layer wrapping and tightening of a flexible material around a fixed spool to securely clutch its inner layer to the spool. When a tensile load is applied to the free end of the flexible material, the outer layers tighten around the inner layers, applying high pressures that clamp the inner layer onto the spool via friction. This results in a sudden increase in tensile load capacity of the spool and self-jamming friction clutching. The overlapping belt friction securely engages the vine robot tip to the spool and bears the load without the need for active grasping. By motorizing the spool to be a winch, the device can also reel in the vine material and disengage the vine robot by winding the spool of the vine material clockwise/counterclockwise.

Both these principles leverage unique characteristics of vine robots, in that the obstacle-aided navigation is enabled by a vine robot's tip growth and compliant body, and clutching via overlapping belt friction is enabled by the vine robot material's inextensibility, high bending flexibility, and frictional properties. In the following sections, we first derive guidelines for selecting geometric parameters for the TCW to allow for the robot tip to grow into in a desirable configuration for the device to secure it to the winch using existing models [6] [7] describing the buckling mechanics of inflated beams. Then, we derive a simplified analytical approximation of the relationship between the holding tension and maximum loading tension for one overlapping layer using Amonton's law of friction. This shows how overlapping belt friction exploits the high tensile strength of the vine robot material.

B. Leveraging Obstacle-Aided Navigation

This section explains how the tip-clutching winch design affects the grown path of the vine robot. Prior work on obstacle-aided navigation [6] illustrates how contacts between the vine robot and its environment determine its trajectory, and demonstrates how the environment can be leveraged to achieve a prescribed path. As shown in Fig. 3b-g, after a vine robot enters the tip-clutching winch, it grows along the inside of the drum wall. The bending moment generated by contact with the wall must be great enough to bend the vine robot around the winch. The vine robot bends due to transverse buckling at discrete points along its length. Haggerty et al. developed a model that relates the transverse buckling conditions for a given vine robot to its configuration within and contact with its environment [7]. Using geometric analysis and this model, we determine the configuration and contact forces of the vine robot with the tip-clutching winch as it everts its outer layer, and define conditional models for the device design to ensure the vine robot can grow through the channel completely.

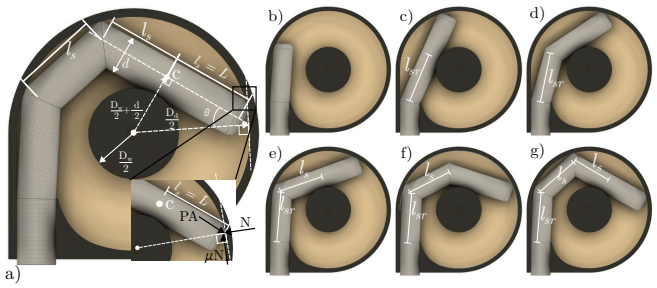

Fig. 3: (a) Diagram of vine robot geometry and tip forces at the moment of buckling (when both ends of the distal segment are colliding with the drum wall). (b-g) Sequence of vine robot growth through the channel showing the formation of segments due to buckling.

Based on Haggerty et al.'s model, the key parameters that determine the transverse buckling conditions are the radius of the vine robot, R, the minimum angle of incidence, θ_{min}, at which it contacts a surface, and the unconstrained length of the vine robot before its tip L. These parameters are related in the free body diagram shown in Fig.3a. Given a vine robot with radius R at an unsupported length L, θ must be greater than θ_{min} for it to buckle, which can be calculated using the following geometric relationship:

$$\frac{R}{L} = \frac{\sin\theta_{\min} - \mu\cos\theta_{\min}}{\cos\theta_{\min} + \mu\sin\theta_{\min}} \tag{1}$$

We ensure that the robot tip is automatically biased to continuously achieve θ_{min} during engagement with the device through careful selection of the geometry of the tip-clutching device's channel. The channel is the gap between the concentric drum and winch walls, and thus its 2D geometry can be simply parameterized as the drum inner diameter D_d and the winch outer diameter D_w. Greer et al. show that vine robots will buckle due to tip contact forces at the most distal point of contact its body has with the environment before its tip (point c in Fig.3a) when the rotation of the segment proximal to that point is constrained. After the vine robot initially buckles at the channel entrance, this buckling point c is always in contact with the winch (Fig 3), and the rotation of the proximal segment is constrained when the previous buckling point collides with the drum wall. Thus, the vine robot configuration relative to the drum and winch walls at the point of buckling can be geometrically defined as shown in Fig.3a. Based on this configuration, the unconstrained segment length L and angle of incidence θ can be defined as:

$$L = \frac{1}{2}\sqrt{D_d^2 - D_w^2 - 4D_w d - 4R^2} \tag{2}$$

and

$$\theta = \sin^{-1}\left(\frac{D_w + 2R}{D_d}\right), \tag{3}$$

respectively. Thus, we can determine whether a given set of drum and winch diameters D_w and D_d for a vine robot with radius R will result in an unsupported length L and angle of incidence θ that satisfies the transverse buckling condition (1).

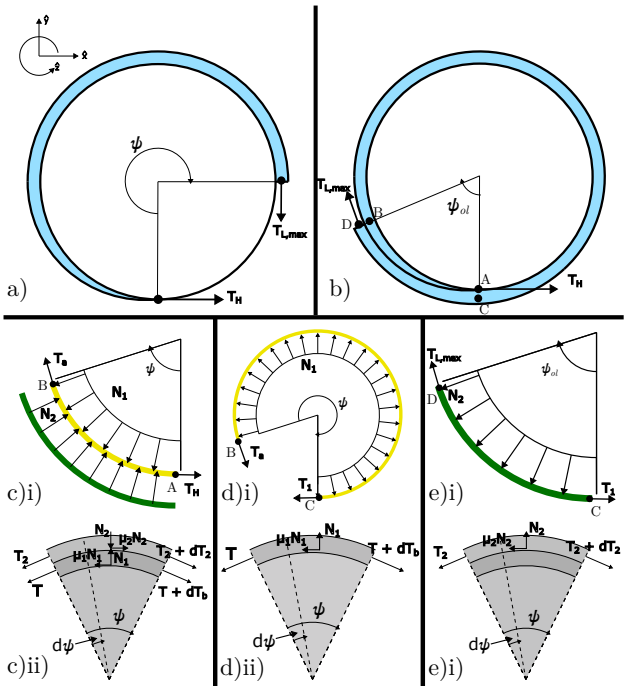

Fig. 4: Standard vs Overlapping Belt Friction. a) Standard Belt Friction Configuration b) Overlapping Belt Friction Configuration. c) inner layer section with overlap $\psi = [0, \psi_{ol}]$ d) inner layer section without overlap $\psi = [\psi_{ol}, 2\pi]$ e) outer layer section causing overlap $\psi = [2\pi, 2\pi + \psi_{ol}]$ i) Sections of the analytical approximation of $T_{L,max}$ vs T_H relationship in overlapping configuration ii) Force equilibrium in a sufficiently small segments of each section

C. Overlapping Belt Friction Clutch Mechanism

The friction between a flexible, inextensible material and a curved object around which it is wrapped determines the relationship between loading tension and holding tension. This relationship is commonly modeled using the Euler-Eytelwein formula [8], better known as the belt friction equation or capstan equation. Our system augments the standard capstan effect in a way that yields a loading tension to holding tension ratio that is significantly higher than typical for the capstan equation. This higher ratio is achieved by the compressive forces of the outer layer of vine material onto the inner layer of vine material which increase the frictional force. [9] [10] [11] have termed this phenomenon as "overlapping belt friction". These works have presented models on the relationship between tensile forces present with overlap and designed non-permanent mechanical locking systems based on it. However, the forces present in our system differ slightly from these works. Therefore, we derived a simplified analytical approximation of the relationship between the holding tension and maximum loading tension for one overlapping layer to describe the effects of the outer layer on the inner layer in our system. As seen in Fig 4b and Fig 4c-d)i), we take a look at sections of the spool configuration and assess each as a static model of a flat belt and modify the capstan derivation based on the internal tensile forces present at the boundaries of each section of the vine robot's material. We evaluate the sections as the contact angle, ψ, between the vine material and the

curved surface beneath it increases in a clockwise direction.

$$T_{L,max}(\psi) = T_H e^{\mu_1 \psi} \tag{4}$$

Prior to our spool of vine material wrapping past 2π around the winch (Fig. 4)a, we effectively have the same scenario as the standard capstan equation (4). T_H is the holding tension applied at $\psi = 0$. For a given T_H, $T_{L,max}$ is the maximum loading tension that can be applied to the capstan and μ_1 is the frictional coefficient between the inner layer material and the winch.

As the spool wraps past 2π, overlap begins and the effects of overlapping belt friction become relevant to the system. Fig. 4b-c shows the forces present for each layer once overlap begins. T_a is the internal tensile force present at $\psi = \psi_{ol}$ where ψ_{ol} is the contact angle along which overlap is present between the outer and inner layer of vine material. T_1 is the internal tensile force present at $\psi = 2\pi(\psi_{ol} = 0)$ where the first wrap around the winch ends and the materials starts to overlap with itself. In the overlapping case, $T_{L,max}$ becomes the loading tension applied to outer layer at $\psi = 2\pi + \psi_{ol}$.

To derive an analytical approximation of the relationship between T_H and $T_{L,max}$ in the overlapping configuration, we begin by considering sufficiently small segments of each section shown in Fig. 4(c-e)i and drawing the free body diagrams in Fig. 4(c-e)ii detailing the tensile forces present at equilibrium in the overlapping area. Building on the small angle approximation established in the capstan equation derivation [8], the static equilibrium equations for the inner layer of material are as given below (5)(6):

$$\Sigma F_x : dT_b - \mu_1 \mathrm{N}_1 \ + \mu_2 \mathrm{N}_2 \tag{5}$$

$$\Sigma F_y : \mathrm{N}_1 - \mathrm{N}_2 - T d\psi \tag{6}$$

where dT_b is the difference in the tensile forces applied at the ends of the segment in the inner layer, $T(\psi)$ is the tension on the left side of the segment, $N_1(\psi)$ is the normal force between the inner layer of the segment and the winch, $N_2(\psi)$ is the normal of the forces between the overlapping segment of the outer and inner layer of material, and μ_2 is the frictional coefficient between the outer and inner layers of the vine material. By solving (6) for N_1, we can substitute it in (5) to get (7)

$$dT_b = \mu_1(\mathrm{N}_2 + T d\psi) \ - \mu_2 \mathrm{N}_2 \tag{7}$$

Equation (6) highlights that introducing the overlapping layer to the belt friction configuration allows N_2 to act as a supplemental radially compressive force on $T(\psi)$. Additionally, (7) suggests that when $\mu_1 > \mu_2$, we observe an instantaneous increase in dT_b from the typical capstan configuration as N_2 is introduced by outer layer from an increase in friction. Both of these phenomena contribute the self jamming friction clutching our device leverages.

Assuming the inner layer is wrapped taut about the winch to the extent that $T_1 = T_{L,max}(\psi = 2\pi)$, we can derive $N_2(\psi)$ by treating the outer layer material as a standard capstan with the inner layer of material being the curved surface it is in contact with as shown in Fig. 4e)i-ii. We draw the relationship expressed by (8) from the derivation of the standard capstan equation [8] and define $T_2(\psi_{ol})$ as $T(\psi = 2\pi + \psi_{ol})$ in (9).

$$N_2(\psi_{ol}) = T_2 d\psi_{ol} \tag{8}$$

In the context of the full configuration of the material, $T_2(\psi_{ol} = 0) = T(\psi = 2\pi) = T_1$ (Fig. 4). Based on our assumptions, $d\psi_{ol} = d\psi$ and $\psi_{ol} = \psi - 2\pi$. Substituting this into (8), we get (9)

$$N_2(\psi) = T_1 e^{\mu_2(\psi - 2\pi)} d\psi \tag{9}$$

Additionally, $N_2(\psi) = 0$ for $\psi = [0, 2\pi]$ and discontinuously becomes (9) after 2π until 4π when a new outer layer is introduced. Substituting (9) into (7), we get the differential equation (10)

$$dT_b = \mu_1(T d\psi + T_1 e^{\mu_2(\psi - 2\pi)} d\psi) - \mu_2(T_1 e^{\mu_2(\psi - 2\pi)} d\psi) \tag{10}$$

Under the assumption of linear friction law (Amonton), a closed form solution(11) relating $T_{L,max}$ to T_H for $T(\psi = [> 2\pi, 4\pi])$ can be obtained by defining T_1 and T_a. σ_1 refers to $\mu_1 - \mu_2$ and σ_2 refers to $2\mu_1 - \mu_2$. Building on the assumption that $T_1 = T_{L,max}(\psi = 2\pi)$, T_1 and T_a can be defined using the standard capstan equation [8] on the inner layer of material as these occur in the range $\psi = [0, 2\pi]$.

$$T_{L,max}(\psi) = e^{\mu_1 \psi}(T_1 + \frac{T_a e^{2\pi(\mu_1 + \sigma_1)} \sigma_1}{\sigma_2}) - \frac{T_a e^{2\pi(\mu_1 + \sigma_1) - \sigma_2 \theta} \sigma_1}{\sigma_2} \tag{11}$$

As the next layer of overlap begins after 4π, we can employ the same approach to define an N_3 referring to the the normal of the forces between the segment of the subsequent outer and inner layers of material that applies for $T(\psi = [> 4\pi, 6\pi])$. In Sec. V, we discuss future works to account for viscoelastic deformation of the vine material which removes the assumption of linear friction law.

III. Design and Implementation

A. Design Considerations

The functional requirements for the tip clutching winch are: (1) engagement, securing, and retraction of an inserted simple vine robot tip, (2) high tensile load capacity, and (3) disengagement of the vine robot tip. We present key design considerations that prevent potential failure modes within the first two requirements. The third requirement, disengagement, is achieved by simply rotating the winch to unwind the vine robot until it is completely unwrapped – there is no expected failure mode for this function.

Engagement of the vine robot is compromised when growth (eversion) stops before the vine robot wraps around

the winch. This occurs when the angle of incidence of the vine robot tip with the drum wall is too large (closer to perpendicular), creating large reaction forces that prevent eversion. The channel width and curvature must be sufficiently large relative to the vine robot diameter such that the tip contact angle is sufficiently close to tangent with the drum wall. Sec. II-B discusses the relationship between the drum and winch designs to angle of incidence. Capstan friction from the internal membrane material sliding within the vine robot, i.e. "tail friction", can also resist eversion [12]. This can be addressed by ensuring that the vine robot burst pressure and diameter (which informs the TCW geometry) are sufficient to generate tip eversion forces capable of overcoming this tail friction.

In the absence of active steering, vine robots grow towards the path of least resistance. Thus, the design of the TCW must ensure that this path leads to the desired configuration within the device. As the vine robot grows further around the winch, its inner layers must grow along the inner curvature of the outer layer and cannot cross over itself. Crossing over, within the context of the TCW, occurs when the vine robot tip grows into the space between the outer layer and the front/back plates of the drum. This is due to either the channel height of the tip clutching device being too high, and/or the vine robot tip angle of incidence with the outer layer being too close to perpendicular.

A channel height greater than the vine robot diameter creates a gap between the outer layer and the side plates, in which the vine robot tip can grow into. Thus, the channel height must be kept small enough relative to the vine robot diameter such that the the vine robot is not biased to cross over. A high heading angle can also cause cross over, as the force pushing normal to the outer layer to be too high relative to the tangential force, thus causing the tip to evert into the outer layer instead of bending along it. This can be caused by the channel being too large and/or the drum diameter being too small, such that the inner layer everts outward in a straight line with a high heading angle when it contacts the outer layer (this relationship is discussed in Sec. II-B.). Thus, the channel width and curvature must be designed such that the tip contact heading angle is kept sufficiently close to tangent.

Additionally, to bias the passive growth of the vine robot into a spool configuration, the vine needs space to grow into its next innermost layer. The inherent compliance of vine robots allows the TCW to leverage the restorative moment present at the inflated beam's buckling point to align the vine toward the drum wall while growing its outermost layer as shown in Fig. 3. However, the friction between the side plates of the device and the vine material needs to be sufficiently minimal for the restorative moment to be effective.

The high tensile load capacity of the clutching mechanism is primarily dependent on the coefficient of friction of the vine robot with the winch and with itself, and the length of the vine robot wrapped around the winch, which is further elucidated in detail in Sec. II.B. Thus, the coefficient of friction of the winch surface material and the channel width, which determines how many times the vine robot can wrap around the winch, are the most relevant design considerations for load capacity. In particular, in order to employ the overlapping belt friction principle that enables the high-strength self-locking clutching behavior of the design framework, the channel width must be greater than the diameter of the vine robot. Otherwise, the vine robot will take up the entire channel space after wrapping around the winch just once, and no space will be left for any subsequent inner layers that the first layer can overlap.

B. Physical System

A prototype of the tip clutching device was developed to implement the previously presented design, as shown in Fig.1. The prototype was designed for a 4.85 cm diameter vine robot. The drum inner radius and winch outer radius were 21.6 cm and 12.7 cm, respectively, yielding a channel width of 8.9 cm, and a theoretical heading angle of $44.5°$ and segment length of 30.81 cm at the buckling point. The radius of curvature of the drum wall's bottom left quadrant was reduced to 17.8 cm to increase the heading angle at which the vine robot tip collides with itself as it completes the outer layer. The channel height was set equal to the vine robot diameter at 4.85 cm. The drum walls and winch were 3D printed using ABS and PLA filaments, respectively. The front and back plates were made of low-friction plastic sheets (clear acrylic lined with UHMW polyethylene film and sanded Delrin® acetal, respectively) to enable the growing vine robot outer layer to bend back toward the drum wall with minimal frictional resistance. A high-torque motor was equipped to the winch for rotation. A small linear actuator with a compliant spring-loaded tip attachment was integrated into the winch to serve as the weak pinching mechanism for the vine robot tip (3.4 N holding force).

IV. Demonstrations and Experiments

A. Automatic Engagement and High-Load Pulling

To validate the design and implementation of our tip clutching device, we performed a demonstration in which a vine robot automatically engaged with the device, was retracted to pull a high load, and then lowered and released from the device (outlined in Fig. 5).

The vine robot body had a diameter of 4.85 cm, was made of 40 denier TPU-coated ripstop fabric, and was pressurized up to 41 kPa (6 psi). A high-strength 3D printed custom fitting with shackle attachments was equipped onto the base of the vine robot to both provide the pressurized air and allow weights to be attached to it without cutting off the air flow through its body. The winch was continuously rotated throughout the demonstration until the vine robot finished growing in order to help the inner layer bend toward the winch during growth. This applied a friction force that pulled the inner side of the inner vine robot layer against its growth direction, which created a small bending force that helped the vine robot follow its path around the winch.

The prototype was successful in automatically engaging, pulling, and disengaging the vine robot without any external

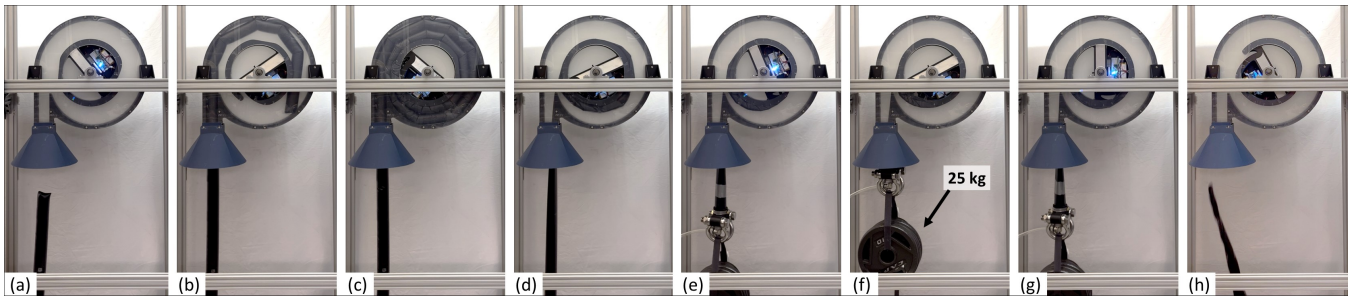

Fig. 5: Demonstration of engagement, pulling, and disengagement of a vine robot with the tip clutching device while bearing a tensile load. The winch continuously rotated counterclockwise during steps (a) through (c) to help bend the vine robot inner layer toward the winch during growth. (a-b) The vine robot grows upwards into the device entrance. (c) The vine robot grows through the channel of the device until the tip fully navigates twice around the winch and into the slot, in which the pinching mechanism is activated to weakly clamp the tip in place (3.4 N holding force). (d) The pressure source is disconnected, and the winch is rotated clockwise to wind up the vine robot into the device and pull on the weights (25 kg) attached to its base. As the vine robot gets tightened around the winch, its body gets flattened and the remaining air gets pushed out. Once it is fully deflated, it gets tightened around the winch, which activates the overlapping friction clutching mechanism to create a strong, secure attachment. (e) The winch continues to wind up the vine robot to lift the weight above the ground. (f) After the weight has been lifted 1 m, the winch stops rotating, and the pinching mechanism is disengaged to demonstrate that the friction clutching mechanism can bear the full load completely independently and passively. (g) The winch then unwinds the vine robot to lower it back onto the ground. (h) The winch continues to unwind until the vine robot is completely unwrapped and falls out of the drum.

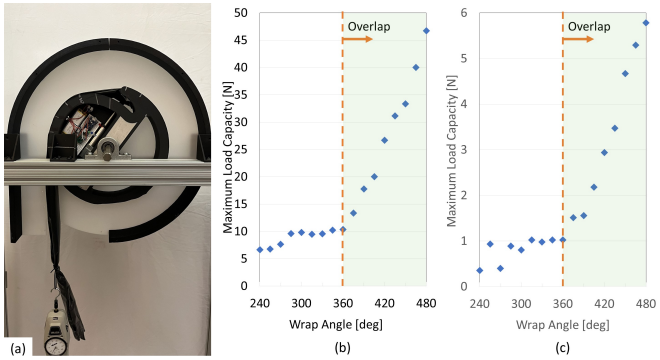

Fig. 6: Load capacity experiments at different wrapping angles. (a) Experimental apparatus. (b) & (c) Experimental results for hold force $T_H = 3.4$ N and $T_H = 0.0$ N, respectively. Once the wrapping angle exceeds 360°, the tensile load capacity increases to higher values than would be expected from standard capstan friction.

physical intervention. The device bore a load of 28.5 kg and lifted 25.08 kg, which is an order of magnitude greater than the previous record of 2.5 kg [3]. These values were limited by the current capacity of the power supply (NICE-POWER DC Variable Power Supply 15V/30A/450W) used to drive the winch motor (AndyMark, Inc 2.5 in. CIM Motor, Inc 100:1 CIM Sport Gearbox).

B. Self-Jamming from Overlapping Belt Friction

To demonstrate the principle of overlapping belt friction via multilayer wrapping, a series of experiments were performed to evaluate the load capacity of the tip clutching device with the vine robot wrapped around the winch at different angles (Fig.6a). Nine experiments were performed with the wrapping angles ranging from 240° to 480°, increasing at intervals of 15°, to specifically observe how the rate of change of the load capacity $T_{L,max}(\psi)$ changes once the vine robot starts to overlap itself. Two T_H conditions at the tip of the vine robot were tested: 0 N and 3.4 N. The 0 N holding tension condition allows us to isolate the effect of the outer layer applying pressure onto the inner layer in our observations. The load capacity was measured using an Imada® MF-2 Analog Force Gauge and Imada® MF-100 Analog Force Gauge. As shown in Fig. 6b, the tensile load capacity started increasing at a much faster rate with respect to the wrapping angle after it exceeded 360°, to higher values than would be expected from standard non-overlapping capstan friction. These results show how the pressure that the tightly wrapped outer layer applies onto the inner layer significantly contributes to the capstan friction and increases the load capacity.

V. Conclusion and Future Work

In this paper, we present a device design that expands the high-tensile force capabilities of vine robots to broaden their range of functionality and potential applications. The design employs obstacle-aided navigation to take advantage of the compliance present in vine robots as well as overlapping belt friction to achieve high pulling forces at least an order of magnitude greater than current tip mount devices in literature. The principles supporting the design are discussed and a demonstration is of the device and the applied principles are presented.

For the sake of simplicity, we utilize Amonton's linear friction law to demonstrate the benefits of overlapping belt friction for the TCW design in Sec. II. However, it has been shown that for textiles and fibrous materials in general which, soft growing robots can be made of, the relationship between frictional force and normal force is given by power law and not linear as it more accurately captures the viscoelastic deformation present for these materials [13] [14]. Equations (4) and (11) simply allow for the definition of an "effective μ" for other models of friction to equate their corresponding results with [9]. The introduction of a non-linear friction model means that (7) will no longer have an analytical solution. In future work, we will further characterize the effect of non-linear friction in the TCW to develop and validate a robust model of the device's maximum force bearing capabilities.

REFERENCES

[1] E. W. Hawkes, L. H. Blumenschein, J. D. Greer, and A. M. Okamura, "A soft robot that navigates its environment through growth," *Science Robotics*, vol. 2, no. 8, p. eaan3028, 2017, dOI: 10.1126/scirobotics.aan3028. [Online]. Available: https://doi.org/10.1126/scirobotics.aan3028

[2] L. H. Blumenschein, M. M. Coad, D. A. Haggerty, A. M. Okamura, and E. W. Hawkes, "Design, modeling, control and application of everting vine robots," *Frontiers in Robotics and AI*, vol. 7, p. 153, 2020. [Online]. Available: https://www.frontiersin.org/article/10.3389/frobt.2020.548266

[3] S. Jeong, M. M. Coad, L. H. Blumenschein, M. Luo, U. Mehmood, J. Kim, A. M. Okamura, and J. Ryu, "A tip mount for transporting sensors and tools using soft growing robots," in *IEEE/RSJ International Conference on Intelligent Robots and Systems*, 2020, pp. 8781–8788. [Online]. Available: https://arxiv.org/abs/1912.08297

[4] M. M. Coad, L. H. Blumenschein, S. Cutler, J. A. R. Zepeda, N. D. Naclerio, H. El-Hussieny, U. Mehmood, J.-H. Ryu, E. W. Hawkes, and A. M. Okamura, "Vine robots: Design, teleoperation and deployment for navigation and exploration," *IEEE Robotics and Automation Magazine*, vol. 27, no. 3, pp. 120–132, 2020. [Online]. Available: https://doi.org/10.1109/MRA.2019.2947538

[5] W. E. Heap, N. D. Naclerio, M. M. Coad, S.-G. Jeong, and E. W. Hawkes, "Soft Retraction Device and Internal Camera Mount for Everting Vine Robots," in *2021 IEEE/RSJ International Conference on Intelligent Robots and Systems (IROS)*, Sep. 2021, pp. 4982–4988, iSSN: 2153-0866.

[6] J. D. Greer, L. H. Blumenschein, R. Alterovitz, E. W. Hawkes, and A. M. Okamura, "Robust navigation of a soft growing robot by exploiting contact with the environment," *The International Journal of Robotics Research*, vol. 39, no. 14, pp. 1724–1738, Dec. 2020, publisher: SAGE Publications Ltd STM. [Online]. Available: https://doi.org/10.1177/0278364920903774

[7] D. A. Haggerty, N. D. Naclerio, and E. W. Hawkes, "Characterizing Environmental Interactions for Soft Growing Robots," in *2019 IEEE/RSJ International Conference on Intelligent Robots and Systems (IROS)*, Nov. 2019, pp. 3335–3342, iSSN: 2153-0866.

[8] M. L. Euler, "Remarque sur l'effet du frottement dans l'quilibre, m moires de l'acado des sc. de berlin," 1762.

[9] P. Schumann, R. Zöllner, and T. Schmidt, "A new model and alternative solutions for the description of double layered flexible elements wrapped around a cylinder," *Mechanism and Machine Theory*, vol. 172, p. 104823, 2022. [Online]. Available: https://www.sciencedirect.com/science/article/pii/S0094114X22000921

[10] N. Matsui, S. Shirafuji, and J. Ota, "Locking mechanism based on flat, overlapping belt, and ultrasonic vibration," in *2016 IEEE International Conference on Robotics and Biomimetics (ROBIO)*, Dec. 2016, pp. 461–466.

[11] S. Shirafuji, N. Matsui, and J. Ota, "Novel frictional-locking-mechanism for a flat belt: Theory, mechanism, and validation," *Mechanism and Machine Theory*, vol. 116, pp. 371–382, Oct. 2017. [Online]. Available: https://www.sciencedirect.com/science/article/pii/S0094114X17306547

[12] L. H. Blumenschein, A. M. Okamura, and E. W. Hawkes, "Modeling of Bioinspired Apical Extension in a Soft Robot," in *Biomimetic and Biohybrid Systems*, ser. Lecture Notes in Computer Science, M. Mangan, M. Cutkosky, A. Mura, P. F. Verschure, T. Prescott, and N. Lepora, Eds. Cham: Springer International Publishing, 2017, pp. 522–531.

[13] X. Gao, L. Wang, and X. Hao, "An improved Capstan equation including power-law friction and bending rigidity for high performance yarn," *Mechanism and Machine Theory*, vol. 90, pp. 84–94, Aug. 2015. [Online]. Available: https://www.sciencedirect.com/science/article/pii/S0094114X15000427

[14] H. Howell, "The general case of friction of a string round a cylinder," *Journal of the Textile Institute Transactions*, vol. 44, no. 8-9, pp. T359–T362, 1953, publisher: Taylor & Francis.